Brush Effects on DNA Chips: Thermodynamics, Kinetics, and Design Guidelines

A. Halperin,* A. Buhot,* and E. B. Zhulina[†]

*UMR 5819 SPrAM (UJF, CNRS, CEA), DRFMC, CEA Grenoble, 38054 Grenoble cedex 9, France; and [†]Institute of Macromolecular Compounds of the Russian Academy of Sciences, 199004 St Petersburg, Russia

ABSTRACT   In biology experiments, oligonucleotide microarrays are contacted with a solution of long nucleic acid targets. The hybridized probes thus carry long tails. When the surface density of the oligonucleotide probes is high enough, the progress of hybridization gives rise to a polyelectrolyte brush due to mutual crowding of the nucleic acid tails. The free-energy penalty associated with the brush modifies both the hybridization isotherms and the rate equations: the attainable hybridization is lowered significantly as is the hybridization rate. When the equilibrium hybridization fraction, x_{eq}, is low, the hybridization follows a Langmuir type isotherm, $x_{eq}/(1 - x_{eq}) = c_t K$ where c_t is the target concentration and K is the equilibrium constant. K is smaller than its bulk value by a factor $(n/N)^{2/5}$ due to wall effects where n and N denote the number of bases in the probe and the target. At higher x_{eq}, when the brush is formed, the leading correction is $x_{eq}/(1 - x_{eq}) = c_t K \exp[-const'(x_{eq}^{2/3} - x_B^{2/3})]$ where x_B corresponds to the onset of the brush regime. The denaturation rate constant in the two regimes is identical. However, the hybridization rate constant in the brush regime is lower, the leading correction being $\exp[-const'(x^{2/3} - x_B^{2/3})]$.

INTRODUCTION

The growing availability of genomic DNA sequences enables research on profiles of gene expression, single nucleotide polymorphism and their role, molecular diagnostics for cancer, etc. In turn, these activities require simultaneous interrogation of a given sample for the presence of numerous different nucleic acid sequences. DNA microarrays, ''DNA chips,'' emerged as an important method for such parallel analysis (1–4). DNA chips function by parallel hybridization of labeled nucleic acid sequences in the solution, known as targets, to an array of nucleic acid probes bound to a surface. Numerous identical probes are localized at a small area known as ''spot'' or ''probe cell.'' The composition of the sample is deduced from the label intensities of the different spots after the hybridization. DNA chips are produced in one of two main formats. In cDNA microarrays, long cDNA targets are physisorbed onto the substrate whereas in oligonucleotide chips short oligonucleotides are chemically bound to the surface via their terminal groups. Our theoretical considerations address the hybridization behavior, kinetics and thermodynamics, of oligonucleotide microarrays when the targets are much longer than the probes as is typically the case in biology experiments (see, for examples, Guo et al. and others (5,6)). In particular, we analyze the consequences of the interactions between the long hybridized targets at the surface (Fig. 1).

A growing theory effort aims to clarify the underlying physics of DNA chips with view of assisting in their design and in the analysis of the results. The Langmuir isotherm and the corresponding kinetic scheme provide a natural starting point for the modeling (7–14) as well as the analysis of the

experimental results (15–23). Within this model, the probes, irrespective of their hybridization state, do not interact. This assumption is justified when the probe density in the spots is sufficiently low. At higher probe densities interactions are no longer negligible and the Langmuir model requires modifications. As we shall discuss, the necessary modifications depend crucially on the length of the targets as characterized by N, the number of bases or monomers. Importantly, in biology experiments the targets are usually significantly longer than the probes. As a result, each hybridized probe binds a long segment of single-stranded nucleic acid formed by the unhybridized part of the target (Fig. 1). This leads to two effects. First, when the tails do not overlap the hybridization at an impenetrable surface incurs an entropic penalty. This reduces the equilibrium constant of hybridization with respect to its bulk value. Second, it is necessary to allow for the crowding of these unhybridized ''tails'' as the fraction of hybridized probes grows. This crowding gives rise to a polymer brush, a phenomenon that was extensively studied in polymer physics (24–26). The theory of polyelectrolyte brushes (26–28), as modified to allow for target-probe interactions and wall effects, enables us to analyze the effects of the crowding on the thermodynamics and kinetics of hybridization on DNA chips. In particular, we obtain the hybridization isotherm and the rate equation in the brush regime when the unhybridized tails overlap. As we shall see, the free-energy penalty associated with the brush gives rise to distinctive modification of the Langmuir isotherm and kinetics. Importantly, the brush penalty reflects both the electrostatic interactions within the probe layer and the entropic price due to the extension of the crowded chains. It results in slower hybridization and lower attainable hybridization.
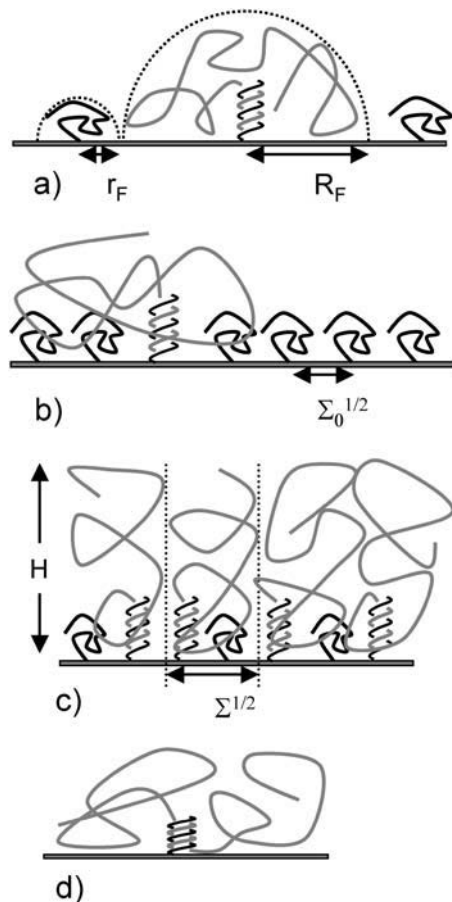
FIGURE 1 A schematic picture of the hybridization of long targets at a layer of short probes. For simplicity we depict the case of targets with a terminal hybridization site, when each hybridized probe carries a long ssDNA tail. Three regimes occur: (a) in the 1:1 regime the distance between the probes, $\Sigma_0^{1/2}$, is large and each hybridized target can only interact with its own probe. There is no crowding of the tails. (b) In the 1:q regime the probe density is higher. At low hybridization fraction each target interacts with $q = R_F^2/\Sigma_0$ probes. (c) As the hybridization fraction increases the hybridized targets begin to crowd each other thus forming a brush with an area per chain $R_F^2 > \Sigma > \Sigma_0$. Note that in the general case the hybridization site is situated roughly in the middle of the target and each hybridized probe carries two tails (d).

Our analysis focuses on oligonucleotide microarrays hybridizing with long targets of single-stranded (ss) DNA. For simplicity we limit the discussion to the experimentally attainable case of monodispersed targets and probes, a passivated surface that eliminates physical adsorption of DNA and probes anchored to the surface via short spacer chains. The qualitative features of our results apply, however, to a wider range of systems. Two hybridization regimes appear, depending on the equilibrium hybridization fraction, x_{eq}, as set by the bulk concentration of the target, c_t. For low x_{eq}, the hybridization isotherm is of the Langmuir form, $x_{eq}/(1 - x_{eq}) = c_t K$, where K is the equilibrium constant of the hybridization reaction at the surface. For probes comprising $n \ll N$ bases, K at an impenetrable surface is reduced by a factor of

$(n/N)^{2/5}$ with respect to the equilibrium constant of the free chains in solution. At higher x_{eq}, obtained at higher c_t, the effective equilibrium constant is modified because of the brush penalty. The leading correction to the hybridization isotherm is $x_{eq}/(1 - x_{eq}) = c_t K \exp[-const'(x_{eq}^{2/3} - x_B^{2/3})]$ where x_B corresponds to the onset of brush formation. The formation of the brush does not affect the denaturation rate constant of the hybridized probe. However, it does lower the hybridization rate constant by a factor of $\exp[-const'(x^{2/3} - x_B^{2/3})]$, where x is the instantaneous hybridization fraction. The proportionality constant scales with $N/\Sigma_0^{2/3}$ where Σ_0 is the area per probe.

To our knowledge, there has been no direct experimental study of the effects of brush formation on the hybridization isotherms and the hybridization rates. Yet, experimental evidence of brush effects has been reported. Guo et al. (5) observed that the maximum attainable hybridization fraction is reached at higher Σ_0 when N increases. Su et al. (29) reported slower hybridization as N increases at fixed Σ_0. A similar effect was reported for RNA targets by Dai et al. (20). Further support for the existence of the brush effect is lent by the widespread use of sample fragmentation to achieve a lower average N (see, for example, Rosenow et al. and others (30,31)).

The practical implications of our analysis concern three issues: the design of DNA chips, the sample preparation, and the analysis of the data. The design of DNA chips currently reflects the view that an increase in the oligonucleotide density in a spot should increase the signal intensity and therefore the sensitivity (32). Certain limitations of this strategy, due to the increase of the DNA diameter upon hybridization and the resulting steric hindrance, has been long recognized (33). In marked distinction, our analysis highlights limitations due to the crowding of the long nonhybridized tails of the targets. Thus, in choosing Σ_0 it is useful to bear in mind the anticipated N of the sample and its effect on the attainable hybridization. When Σ_0 is fixed, our analysis provides guidelines for the sample preparation. In particular, the choice of N as determined by the polymerase chain reaction (PCR) primers or the fragmentation procedure. Concerning data analysis, our discussion identifies possible sources of error when comparing spot intensities of samples with different N. These may occur because both the onset of saturation and the hybridization rate vary with N. In quantitative terms, our analysis yields two guidelines: Concerning equilibrium hybridization, it leads to a simple relationship between the area per probe, Σ_0, the number of bases in the probe, n, the number of bases in the target, N, and the attainable sensitivity as measured by c_{50}, i.e., the target concentration resulting in 50% hybridization at the spot. Regarding the kinetics, it yields a simple criterion for the onset of slowdown due to the brush formation.

Experiments using DNA chips involve many control parameters concerning the chip design, the sample preparation, and the hybridization conditions. These are outlined in

''Design of oligonucleotide microarray experiments'' together with a discussion of the resulting hybridization regimes and the choice of parameters used in our numerical calculations. Our analysis incorporates ingredients from the theory of polymer brushes. These are summarized in ''Background on polymer brushes''. This section describes the Flory version of the Alexander model of brushes as applied to terminally anchored polyelectrolytes in aqueous solution of high ionic strength. The model is modified to incorporate the effect of an impenetrable grafting surface. This is important to ensure crossover to the mushroom regime of nonoverlapping tails, and to enable comparison of the hybridization constants at the surface and in the bulk. Because the hybridization site is typically situated within the target, each hybridized probe carries two unhybridized tails. The necessary modifications are also discussed. When brush formation is possible, the hybridized targets also interact with neighboring probes. The resulting free-energy penalty, within the Flory approximation, is described in ''Target-Probe Interactions''. The free energies associated with the brush and with the target-probe interactions enable us to obtain the equilibrium hybridization isotherms. The derivation is discussed in ''Brush effects: thermodynamics of hybridization''. The hybridization isotherms allow us to quantify the sensitivity in terms of the corresponding c_{50}'s. In turn, these yield design guidelines relating the sensitivity to n, N, and Σ_0. Assuming, and later checking, that the hybridization rate at the surface is reaction controlled enables us to specify the hybridization and denaturation rate constants in the different regimes. The necessary background, on the hybridization kinetics in the bulk and the desorption dynamics out of a brush, as well as the resulting rate equations are discussed in "Brush effects: kinetics of hybridization". The second virial coefficient, v, specifying the interactions between the charged monomers of polyelectrolytes in the high-salt regime is discussed in Appendix A. Using this v, we recover our earlier results of the $n = N$ case and discuss the comparison to the $N \gg n$ scenario. In Appendix B we present an alternative derivation of our result for the hybridization constant in the low surface density regime. This utilizes exact results, thus avoiding the approximations inherent in the ''Alexander-Flory'' approximation.

DESIGN OF OLIGONUCLEOTIDE MICROARRAY EXPERIMENTS

Oligonucleotide chip experiments vary widely in their design. A brief summary of the possible designs is necessary to delineate the range of applicability of our analysis and the different possible regimes. To this end it is helpful to distinguish between three groups of design parameters: the chip design, the sample characteristics, and the hybridization conditions. The primary parameters in the chip design are the area per probe, Σ_0, and the number of bases in the probe, n (32); n values in the range 10–60 are typical. In this context

one should discriminate two approaches to the production of oligonucleotide chips. In one, the probes are synthesized in situ using photolithography or ink jet technology. In the other, presynthesized oligonucleotides with functionalized end groups are delivered to the spot. In the first approach it is necessary to allow for the production of incomplete sequences leading to polydispersity in n (15). The reported probe densities within spots vary between 1.2×10^{10} and 4×10^{13} probes per cm^2 corresponding to $2.5 \times 10^2 \text{Å}^2 \leq \Sigma_0 \leq 8.3 \times 10^5 \text{Å}^2$. The chip characteristics also include the nature of the surface treatment used to minimize nonspecific adsorption and of the spacer chains joining the probe to the anchoring functionality (length, charge, hydrophobicity, etc.).

A key qualitative characteristic of the sample is the chemical nature of the targets (1,3,4). To begin, it is necessary to distinguish between DNA and RNA targets, which differ in two respects: first, single-stranded (ss) RNA exhibits a pronounced secondary structure (loops, hairpins, etc.) that is largely absent in ssDNA. Second, the hybridization free energy of RNA-DNA complexes is higher than that of DNA-DNA ones. For DNA samples, it is further necessary to distinguish between samples of double-stranded (ds) DNA, as obtained from symmetric PCR amplification, and ssDNA samples as obtained, for example, using Lambda exonuclease digestion. The hybridization isotherms of the two types of samples are different (13). The labeling of the targets can also affect the hybridization behavior (34). Our discussion concerns samples of ssDNA targets assuming ideal labels that do not interfere with the hybridization. It focuses on the role of two quantitative characteristics of the sample: the number of bases in the target, N, and the molar concentration of the target, c_t. N is determined by the choice of primers used for the PCR amplification or by the fragmentation step in the sample preparation. Note that the products of the PCR are monodisperse whereas the fragmentation introduces polydispersity in the size of the targets. In this last case it is only possible to control the average size of the targets. Typical reported values for PCR products vary in the range $100 \leq N \leq 350$. The average N resulting from the fragmentation procedure is not always specified but the range $50 \leq N \leq 200$ is representative. It is useful to note another distinction between the two procedures. Targets produced by PCR often have the hybridization site situated roughly in the middle of the target. In the case of fragmented targets, the location of the hybridization site is no longer controlled. With regard to c_t it is helpful to stress the distinction between bioanalytic experiments, utilizing DNA chips to interrogate biological samples (see, for example, Prix et al. (6)), and physical chemistry experiments aiming to understand the function of DNA chips (see, for example, Peterson et al. (22)). In biology experiments c_t is a priori unknown because it is set by the biological sample and its treatment. In marked contrast, in physical chemistry experiments the target concentration is imposed by the experimentalist as is the composition of the sample. In such

experiments the target used is often identical in length to the probes, $n = N$. As noted earlier, our analysis is motivated by bioanalytical experiments where $N \gg n$.

The hybridization conditions include the composition of the hybridization solution, the hybridization temperature, T, and the hybridization time, t_h. Typical hybridization temperatures vary over the range $30°C \leq T \leq 60°C$ depending on n and the GC fraction. The hybridization times also vary widely with typical values in the range of $2h \leq t_h \leq 16h$. In most cases the hybridization solution contains 1 M of NaCl.

Different hybridization regimes are possible, depending on the values of n, N, and Σ_0. To distinguish these regimes, it is necessary to first specify the molecular length scales of ssDNA and dsDNA. These are well established for dsDNA (35). In the range of parameters considered, dsDNA is a rod-like molecule with each basepair contributing 3.4 Å to its length. The radius of dsDNA is 9.5 Å and its cross-section area is 284 Å^2. We will limit our analysis to $\Sigma_0 > 284$ Å^2 to avoid discussion of steric hindrance to hybridization. The corresponding characteristics of ssDNA are not well established. A typical value of the monomer size is $a = 6$ Å (36,37). The cited values of the persistence length, l_p, vary between $l_p = 7.5$ Å and $l_p = 35$ Å (38). ssDNA is often described as a random coil though long-range interactions are expected to give rise to swollen configurations (39). In the following we will consider ssDNA as a swollen coil characterized by its Flory radius (40). This choice is dictated by our treatment of the brush, where the Flory radius emerges as a natural length scale. Accordingly, an isolated unhybridized probe occupies a hemisphere of radius $r_F \sim n^{3/5}a$ whereas a terminally hybridized target occupies a hemisphere of radius $R_F \sim (N - n)^{3/5}a \simeq N^{3/5}a$. As we shall discuss, the unhybridized probes do not interact when $r_F^2 < \Sigma_0$. Similarly, when $R_F^2 < \Sigma_0$ there is no brush regime. It is thus possible to distinguish between three different scenarios. A Langmuir regime is expected when $\Sigma_0 > R_F^2 > r_F^2$. Brush effects, with no interactions between the probes, will occur when $r_F^2 < \Sigma_0 < R_F^2$. Finally, when $\Sigma_0 < r_F^2 < R_F^2$ both the brush effect and probe-probe interactions play a role. All three scenarios occur in the reported variety of DNA chips.

In the following we consider the role of n, N, and Σ_0 in bioanalytical experiments. For brevity we focus on the simplest among the experimentally realistic situations. Thus, we consider monodispersed ssDNA targets and monodispersed oligonucleotide probes. This avoids complication due to unspecified polydispersity and to competitive bulk hybridization. It is convenient to concentrate on the $r_F^2 < \Sigma_0 < R_F^2$ case with $N \gg n$. As we shall see, this makes for a simpler discussion of the brush effects. It also allows us to ignore small corrections due to probe-probe interactions. Finally, our analysis assumes DNA chips with a passivated surface and probes anchored to the surface via short, flexible spacer chains.

Our analysis is concerned with the modifications of the hybridization isotherm and rate equations as Σ_0 decreases

from the Langmuir range, $\Sigma_0 > R_F^2 > r_F^2$, into the brush regime, $r_F^2 < \Sigma_0 < R_F^2$. To implement this program, it is helpful to identify a reference state. In the following we utilize a probe layer that approaches the bulk values for the hybridization rate and equilibrium constants. We argue that this is the case when the following conditions are satisfied. First, the surface is perfectly nonadsorbing to both ss- and dsDNA. Under these conditions adsorbed states are not involved in the hybridization reaction and the two-state approximation for the hybridization reaction is justified. Second, the probes are attached to the surface via long, flexible, and neutral spacers. We argue that the effect of the surface diminishes as the length of the spacers increases. Note that the spacers modify two effects. One is the steric hindrance that occurs when the probes are directly attached to the surface. The other is the reduction in the number of accessible configurations in the vicinity of an impenetrable planar surface. Ideally, the reference state involves spacer chains that do not interact with either the probes and the targets. The third condition is that the distance between the anchored probes ensures zero probe-probe interaction energy, irrespective of their hybridization state. For this reference state, the equilibrium hybridization constant at the surface K_{pt} approaches $K_{\bar{p}t}$, the equilibrium hybridization constant for the bulk reaction between the free chains. Accordingly, the hybridization isotherm in the small spot limit, when the hybridization at the surface has a negligible effect on initial molar concentration of the target c_t, is

$$\frac{x_{eq}}{1 - x_{eq}} = K_{pt}c_t. \qquad (1)$$

It is important to distinguish between K_{pt} and

$$K_{pt}^0 = \exp\left(-\frac{\Delta G_{pt}^0}{RT}\right), \qquad (2)$$

where ΔG_{pt}^0 is the molar standard hybridization free energy as obtained from the nearest neighbor model (41), T is the temperature, and $R = 1.987$ cal/mol.K is the gas constant. First, K_{pt}^0 and ΔG_{pt}^0 as calculated from the nearest-neighbor model are identical for all $N \geq n + 2$. They allow, at most, for the effect of two dangling ends. Second, this model incorporates only nearest-neighbor interactions along the backbone of the chain. It thus assumes that the oligonucleotide adopts the configuration of an ideal random coil. In particular, ΔG_{pt}^0 does not account for excluded volume interactions between the monomers. In addition, ΔG_{pt}^0 clearly does not allow for the effect of the impenetrable wall or for the interactions between the hybridized targets or between them and the neighboring probes. These additional terms and their effect on the hybridization isotherm will be discussed in the following three sections.

Our choice of the parameters used in the numerical calculations is based on two experimental systems. One, of Guo et al. (5), utilized probes of length $n = 15$ with PCR

produced targets of length $N = 157$ or 347. Both ssDNA and dsDNA were investigated, the area per probe was varied in the range $300 \text{ Å}^2 \leq \Sigma_0 \leq 3000 \text{ Å}^2$, and the hybridization was carried out at $T = 30°C$. The hybridization times varied with N being $t_h = 2$–3 h for $N = 157$ and $t_h = 6$–8 h for $N = 347$. Note that in this study some of the data corresponds to the $\Sigma_0 < r_F^2 < R_F^2$ regime where probe-probe interactions are not negligible. The second system is the Affymetrix Gene-Chip *Escherichia coli* antisense genome array (31). In this case, probes of length $n = 25$ hybridize with fragmented, thus polydispersed, ds cDNA targets with average length in the range $50 \leq N \leq 200$. The hybridization is carried out at $T = 45°C$ for $t_h = 16$ h. A rough approximation of Σ_0 for Affymetrix chips was obtained from the estimated density of functional groups in the substrate before the synthesis of the probes: 27 pM/cm^2, and the stepwise yield of the synthesis, $\sim$90%. Only 14 pM/cm^2 attain $n \geq 6$ (15). This estimate yields $\Sigma_0 \geq 1200 \text{ Å}^2$. In both systems the hybridization was carried out in a solution containing 1 M of NaCl. The base sequence of the probes considered in the calculations and their thermodynamic parameters for hybridization, as calculated using the nearest-neighbor model with a perfectly matched target (42–44), are specified in Table 1.

BACKGROUND ON POLYMER BRUSHES

Polymer brushes are formed by chains with one monomer anchored to a planar surface (24,25). In the simplest case, the anchoring moiety is the terminal monomer. When the area per chain, Σ, is large the chains do not crowd each other. In this ''mushroom'' regime, the chains may be roughly considered as occupying hemispheres whose radius is comparable to the Flory radius of the free chain, R_F. When the surface density increases such that $\Sigma \leq R_F^2$, the chains begin to crowd each other, thus forming a ''brush''. In the brush regime the chains stretch out along the normal to the surface so as to decrease the monomer concentration, c, and the

TABLE 1 The thermodynamic parameters utilized in the numerical calculations

Probe	ΔH_{pt}^0 kcal/mol	ΔS_{pt}^0 cal/mol.K	$\Delta G_{pt}^0(30°C)$ kcal/mol	$\Delta G_{pt}^0(45°C)$ kcal/mol
$p1$	−121.00	−334.06	−19.73	−14.72
$p2$	−203.30	−546.32	−37.69	−29.49

Parameters correspond to two probes: i), the $n = 15$ wild-type probe $p1$ (5′–*CGTCCTCTTCAAGAA*–3′) incorporates the codon 406 of exon 4 of the human tyrosinase gene. The $N = 157$ and 347 targets incorporate the perfect complementary segment 5′–*TTCTTGAAGAGGACG*–3′ (5). ii), The Affymetrix *E. Coli* antisense $n = 25$ probe $p2$ annotated AFFX-BioB-5_at:242:77, with interrogation point 177, corresponds to the sequence 5′–*AGATTGCAAATACTGCCCGCAAACG*–3′. The fragmented cDNA targets incorporate the perfect complementary sequence 5′–*CGTTTGCGGGCAG-TATTTGCAATCT*–3′. The parameters are calculated from the nearest-neighbor model (42–44) using the HyTher program with a 1 M NaCl salt concentration. Because the targets are longer than the probes two dangling ends are invoked.

number of repulsive monomer-monomer contacts. A simple description that captures the leading behavior of brushes is provided by the Alexander model (24,25,45). Within it the concentration profile of the brush is modeled by a step function of height H, i.e., $c = N/H\Sigma$ at altitudes up to H above the surface and $c = 0$ for higher altitudes. All the free ends are assumed to straddle the outer boundary of the brush at height H. In the following we will use the Flory version of the model, ignoring scaling corrections. The regime of validity of this mean field approach for semiflexible chains is expanded in comparison to that of flexible polymers (46). This justifies the use of the ''Alexander-Flory'' model with a free energy per chain in a brush

$$\frac{G}{kT} = v\frac{N^2}{\Sigma H} + \frac{H^2}{Nal_p} - \ln\frac{H}{Na}, \tag{3}$$

where k is the Boltzmann constant. The first term allows for the monomer-monomer interactions. It is of the form vc^2V_{chain} where v is the second virial coefficient and $V_{chain} = \Sigma H$ is the volume per chain. The second accounts for the entropy loss incurred because of the stretching of a Gaussian chain, comprising of Na/l_p persistent sequences of length l_p, along the normal to the surface. Here a is the monomer size, l_p is the persistence length of the chain, and the span of the Gaussian unswollen coil is $R_0 = \sqrt{Nal_p}$. The last term arises because the impenetrable surface carrying the anchoring site reduces the number of accessible configurations of the tethered chain. For a Gaussian chain with a free end at altitude H the number is reduced by a factor of Hl_p/R_0^2 (47). This contribution is often ignored because it has a negligible effect on the equilibrium dimensions of the chains. It leads, however, to a significant modification of the hybridization constant at the surface. The last two terms of Eq. 3 apply, in this form, when $Na \gg l_p$. We have omitted a term allowing for the entropy associated with the placement of the free end. This is because the Alexander model assumes that all free ends are constrained to the brush boundary. For simplicity we ignore, here and in the following, numerical factors of order unity. Minimization of G with respect to H yields the equilibrium values of G_{brush} and H

$$\frac{G_{brush}}{kT} = N\left(\frac{a^2}{\Sigma}\right)^{2/3}\left(\frac{a}{l_p}\right)^{1/3}\left(\frac{v}{a^3}\right)^{2/3}$$
$$- \ln\left[\left(\frac{a^2}{\Sigma}\right)^{1/3}\left(\frac{l_p}{a}\right)^{1/3}\left(\frac{v}{a^3}\right)^{1/3}\right], \tag{4}$$

$$\frac{H}{a} = N\left(\frac{a^2}{\Sigma}\right)^{1/3}\left(\frac{l_p}{a}\right)^{1/3}\left(\frac{v}{a^3}\right)^{1/3}. \tag{5}$$

In the mushroom regime, the chains occupy a hemisphere of radius

$$\frac{R_F}{a} = N^{3/5}\left(\frac{l_p}{a}\right)^{1/5}\left(\frac{v}{a^3}\right)^{1/5}. \tag{6}$$

Accordingly, the free energy per chain in the mushroom regime, G_{mush}, is set by the requirement $G_{mush} = G_{brush}$ at the mushroom-brush boundary when $\Sigma = R_F^2$ and $H = R_F$ thus leading to

$$\frac{G_{mush}}{kT} = N^{1/5} \left(\frac{a}{l_p}\right)^{3/5} \left(\frac{v}{a^3}\right)^{2/5} - \ln \left[N^{-2/5} \left(\frac{l_p}{a}\right)^{1/5} \left(\frac{v}{a^3}\right)^{1/5}\right]. \quad (7)$$

As noted earlier, the properties of the chains in the mushroom regime are comparable to those of free coils. In turn, the free coil behavior is specified by the free energy (48)

$$\frac{G}{kT} = v\frac{N^2}{r^3} + \frac{r^2}{Nal_p}, \quad (8)$$

leading, upon minimization with respect to the radius r, to R_F as given by Eq. 6 and to the equilibrium free energy of a coil

$$\frac{G_{coil}}{kT} = N^{1/5} \left(\frac{a}{l_p}\right)^{3/5} \left(\frac{v}{a^3}\right)^{2/5}. \quad (9)$$

The difference between G_{mush} and G_{coil} is due to the logarithmic correction $-\ln(R_F/Na)$ arising from the wall effect.

Within the approach described above, the nature of the grafted chain is specified by three parameters, the monomer size a, the persistence length l_p, and the second virial coefficient associated with monomer-monomer interactions v. For the case of a brush formed by polyelectrolyte chains in aqueous solution of high ionic strength, "high salt," v can be approximated (see Appendix A and Pincus (27)) by

$$v = \frac{2\pi}{3} a^3 \left(1 - \frac{\theta}{T}\right) + 2\pi l_B r_D^2. \quad (10)$$

The first term allows for the hard core repulsion between the monomers and for a weak, long-ranged van der Waals attraction between them. Here θ is the θ-temperature where v of a neutral chain vanishes, thus leading to the behavior of an ideal Gaussian coil. This term by itself is used to describe the behavior of neutral polymers (40). The second term arises from the screened electrostatic interactions between the singly charged monomers. Here $l_B = e^2/\epsilon kT$ is the Bjerrum length (49) where ϵ is the dielectric constant, k the Boltzmann constant, and T the temperature. In water, with $\epsilon \simeq 80$ at room temperature, $l_B \simeq 7$ Å. Note that the variation of ϵ with T contributes to the T dependence of l_B. The Debye length r_D characterizes the range of the screened electrostatic interactions in a salt solution (49). For a 1:1 salt with number concentration of ions c_s, $r_D = 1/\sqrt{8\pi l_B c_s}$ thus, in a 1-M solution $r_D = 3$ Å. In our model, the presence of the $2\pi l_B r_D^2$ term in v distinguishes polyelectrolyte brushes from neutral ones. It is important to stress the limitations of approximating v by Eq. 10. It corresponds to the interactions between individual charged spherical monomers. For cylindrical noncharged monomers $v \simeq l_p^2 a$ rather than

$v \simeq a^3$ (40). Furthermore, this description does not allow for the contribution of hydrogen bonds with water nor for the effect of correlations on the electrostatic interactions. Finally, the appropriate θ temperature remains to be determined. With these caveats in mind, the second term is roughly comparable to $2\pi a^3/3$ and should be dominant for $T \gtrsim \theta$. As a result v is comparable to $2\pi a^3/3$ and the swelling behavior of the chain is similar to that of a neutral chain in an athermal solvent (48). In other words, even short chains swell to their Flory radius. We should add that by using $v \simeq 2\pi l_B r_D^2$ we are able to recover our earlier results (13) for the case of $n = N$ (Appendix A).

In the Flory-type approach, described above, the equilibrium state is determined by a global balance of the osmotic pressure of the monomers and the restoring elastic force of the stretched Gaussian chains. A more refined analysis of the brushes, utilizing self-consistent field (SCF) theory, is possible. This avoids the assumptions of uniform stretching and step-like concentration profiles. It yields the same functional forms for the characteristic height, H, and for G_{brush} but with somewhat different numerical prefactors. With these reservations in mind we utilize the simplest approach, described earlier, because it typically yields the correct leading behavior in similar systems. A SCF theory is necessary for the description of effects that depend strongly on the details of the concentration profile and the distribution of the free ends.

Our discussion thus far concerned brushes anchored to the surface by the terminal headgroup. In DNA chips the situation is often different in that the hybridization site, the anchoring functionality, is located roughly at the middle of the target. As a result, each hybridized probe carries two unhybridized tails (Fig. 1 d) of length N_1 and $N_2 = N_1(1 + \alpha)$ such that $N_1 + N_2 + n = N$. In considering the effect of this feature note that in the brush regime the details of the anchoring functionality are screened with a distance $\Sigma^{1/2}$ from the surface. As a result, it is possible to estimate the modification of G_{brush} and H in two cases, $N_1 = N_2 \gg n$ and $N_2 \gg N_1 \gg n$. When $N_1 = N_2$ the resulting brush is similar to that formed by chains of length $N/2$ but with an area per chain $\Sigma/2$. In this case G_{brush} is larger by a factor $2^{2/3} \simeq 1.6$ whereas H is smaller by a factor $2^{2/3}$ in comparison to the values found for a brush of terminally anchored chains of length N and area per chain Σ. In the limit of $N_2 \gg N_1 \gg n$ the resulting brush may be considered as bidispersed, comprising an equal number of chains of length N_1 and N_2. Such a bidispersed brush can be described as a superposition of two brushes (50). A simple two-layer model incorporates an inner brush of chains of length N_1 and area per chain of $\Sigma/2$ and an outer brush formed by chains of length $N_2 - N_1 = \alpha N_1$ and area per chain Σ at the distal boundary of the inner brush. Within the Flory approximation this scheme leads to $\tilde{G}_{brush} = ((\alpha + 2^{5/3})/(\alpha + 2))G_{brush}$ and $\tilde{H} = ((\alpha + 2^{1/3})/(\alpha + 2))H$ where G_{brush} and H correspond to a monodispersed brush of chains of length N with an area per chain Σ. Note that $\alpha = 0$ corresponds to $N_1 = N_2$ whereas

$\alpha \gg 1$ to $N_2 \gg N_1$. In both cases the effect is to modify G_{brush} and H as obtained earlier by a multiplicative factor of order unity. In keeping with our policy we will omit these numerical factors in the interest of simplicity.

TARGET-PROBE INTERACTIONS

The preceding discussion of brushes allows for the inter-actions among the hybridized targets and the effects of the impenetrable wall. However, the brush regime is only attainable when the hybridized targets can interact with neighboring probes, thus giving rise to an additional con-tribution to the free energy of the system. In discussing the target-probe interactions it is useful to distinguish between three regimes. When $\Sigma_0 > R_F^2 > r_F^2$ the hybridized targets cannot crowd each other. Roughly speaking, each one may be considered to occupy a hemisphere of radius R_F con-taining a single probe that is hybridized to the target (Fig. 1 a). Because each target interacts with a single probe we will refer to this regime as 1:1. Our principle interest is in the two regimes that occur when $R_F^2 > \Sigma_0 > r_F^2$. When the hy-bridization degree x is sufficiently small each target will occupy, as before, a hemisphere of radius R_F. However, it will now interact with $q = R_F^2/\Sigma_0$ probes (Fig. 1 b). We will thus refer to this regime as 1:q. Note that in the polymer science nomenclature both 1:1 and 1:q regimes fall into the ''mushroom'' range, when the tethered chains do not over-lap. The brush threshold occurs at $x = x_B$ when the hemi-spheres occupied by the different targets come into grazing contact. For a surface of total area A_T the area per hybridized target is $\Sigma = A_T/xN_T = \Sigma_0/x$ where N_T is the total number of probes; x_B corresponds to $\Sigma = R_F^2$ or $x_B = \Sigma_0/R_F^2 = 1/q$. When x exceeds x_B the hybridized targets begin to overlap, thus forming a brush (Fig. 1 c). Because the area per chain in this regime decreases as $\Sigma = \Sigma_0/x$ the target experiences interactions only with $x^{-1} < q$ probes.

To estimate the free energy of interactions between the target and the probes, in the spirit of the Flory approach, we assume that each probe contributes an interaction free energy $G_{int}/kT = vnc$. Here c is the monomer concentration within the monomer cloud formed by the hybridized targets, i.e., we assume the interaction with the probes does not affect c as obtained in our earlier discussion of the mushroom and brush regimes. As we shall elaborate later, this assumption is justified only when $G_{int} \ll G_{coil}(N)$ or

$$\Sigma_0 \gg N^{1/5} n a^2 \left(\frac{l_p}{a}\right)^{2/5} \left(\frac{v}{a^3}\right)^{2/5}. \quad (11)$$

In the 1:1 regime each hybridized target occupies a hemisphere of radius R_F incorporating a single probe. Accordingly $G_{int}^{1:1}/kT = vnc$ with $c = N/R_F^3$, thus leading to

$$\frac{G_{int}^{1:1}}{kT} = \frac{n}{N^{4/5}} \left(\frac{a}{l_p}\right)^{3/5} \left(\frac{v}{a^3}\right)^{2/5}. \quad (12)$$

This estimate is reasonable when $N \gg n$ such that the region occupied by the unhybridized target is sufficiently large so as to encompass the hybridized probe. Roughly speaking, this implies $(N - n)^{3/5}a > 3.4n$ Å. Within the 1:q regime each hybridized target interacts with $q = R_F^2/\Sigma_0$ probes. Accord-ingly $G_{int}^{1:q}/kT = v(R_F^2/\Sigma_0)nc$ with $c = N/R_F^3$ or

$$\frac{G_{int}^{1:q}}{kT} = N^{2/5} n \left(\frac{a^2}{\Sigma_0}\right) \left(\frac{a}{l_p}\right)^{1/5} \left(\frac{v}{a^3}\right)^{4/5}. \quad (13)$$

$G_{int}^{1:1}$ and $G_{int}^{1:q}$ are independent of x. In marked contrast G_{int}^{B}, accounting for the target-probe interactions in the brush regime, varies with x. This variation arises because of the x dependence of the monomer concentration within the brush, $c_{brush} = N/\Sigma H$ where $\Sigma \sim 1/x$ and $H \sim x^{1/3}$. $G_{brush}(x)$ is obtained from Eq. 4 upon replacing Σ by Σ_0/x. Within the Flory approach the total interaction free energy between the targets and the probes is vN_Tnc_{brush}. The interaction free energy per hybridized target is thus vnc_{brush}/x or

$$\frac{G_{int}^{B}}{kT} = \frac{vnN}{\Sigma_0 H} = nx^{-1/3} \left(\frac{a^2}{\Sigma_0}\right)^{2/3} \left(\frac{a}{l_p}\right)^{1/3} \left(\frac{v}{a^3}\right)^{2/3}. \quad (14)$$

The condition Eq. 11 ensures that the interaction term $G_{int}^{1:q}$ is a weak perturbation to the Flory free energy of the mushroom $G_{mush}(N)$. When this requirement is not satisfied the chain span exceeds the Flory radius. This is an unphysical result because the interactions driving the extra swelling are confined to the surface. In this case the chain can no longer be assumed to occupy a hemispherical region encompassing the probes. The uniform monomeric distribution inherent to the Flory approach should be refined so as to reflect locally stretched configurations allowing the chain to avoid the probes. For simplicity we will not consider this regime.

BRUSH EFFECTS: THERMODYNAMICS OF HYBRIDIZATION

Having obtained the free-energy terms associated with target-target and target-probe interactions at the surface, we are in a position to investigate their effect on the hybridization iso-therm. To simplify the equations we set $v = a^3$ and $l_p = a$. The hybridization isotherm is determined by the equilibrium con-dition of the hybridization reaction $p + t \rightleftharpoons pt$ at the probe layer that is, $\mu_{pt} = \mu_p + \mu_t$ where μ_i is the chemical potential of species i. Here p and t signify single-stranded probe and target whereas pt is the hybridized probe-target pair. We first consider μ_t. In practice, the molar concentration of the targets, c_t, is only weakly diminished by the hybridization reaction and it is reasonable to assume that c_t is constant. The generalization to the opposite case, when this small spot approximation fails, is straightforward (13). Because the target solution is dilute and the ionic strength of the solution is high, electrostatic interactions between the targets are screened. Consequently μ_t assumes the weak solution form

$$\mu_t = \mu_t^0 + N_{Av}G_{coil}(N) + RT \ln c_t, \quad (15)$$

where μ_t^0 is the chemical potential of the standard state of the hybridization site and N_{Av} is the Avogadro number. We choose a standard state such that $\mu_{pt}^0 - \mu_p^0 - \mu_t^0 = \Delta G_{pt}^0$ as given by the nearest-neighbor method. As discussed earlier, this implies a standard state having an ideal coil configuration. When the hybridization site is within the target, it also reflects the contribution of two dangling ends. $G_{coil}(N)$, as given by Eq. 7, allows for the swelling of the free coil due to excluded volume and electrostatic interactions. Strictly speaking, $\mu_t = \mu_t^0 + N_{Av} G_{coil} + RT \ln a_t$ where a_t is the activity (51). The dimensionless a_t is related to the molar concentration of targets c_t via $a_t = \gamma c_t$ where γ is the activity coefficient. Because $\gamma \to 1$ as $c_t \to 0$ we will, for simplicity, express μ_t by Eq. 15 noting that the molar c_t in this expression is dimensionless.

It is useful to first specify K_{pt} of the reference state corresponding, as discussed in ''Design of oligonucleotide microarray experiments'', to $K_{\bar{p}t}$ of the bulk reaction $\bar{p} + t \rightleftharpoons \bar{p}t$ where $\bar{p}$ denotes a free probe chain. To this end we need

$$\mu_{\bar{p}} = \mu_p^0 + N_{Av} G_{coil}(n) + RT \ln c_{\bar{p}}, \qquad (16)$$

and

$$\mu_{\bar{p}t} = \mu_{pt}^0 + N_{Av}[G_{coil}(N - n) + G_{int}^{1:1}] + RT \ln c_{\bar{p}t}. \qquad (17)$$

The equilibrium condition $\mu_t + \mu_{\bar{p}} = \mu_{\bar{p}t}$ yields $K_{\bar{p}t} = K_{pt}$ with

$$K_{pt} = \exp\left\{ -\frac{\Delta G_{pt}^0 + N_{Av}[G_{coil}(N - n) + G_{int}^{1:1} - G_{coil}(n) - G_{coil}(N)]}{RT} \right\} = K_{pt}^0 \exp\left[n^{1/5} - \frac{n}{N^{4/5}} \right], \qquad (18)$$

where $K_{pt}^0 = \exp(-\Delta G_{pt}^0 / RT)$ and $\Delta G_{pt}^0 = \mu_{pt}^0 - \mu_p^0 - \mu_t^0$. $K_{pt} > K_{pt}^0$ because the hybridization results in the formation of a rodlike ds domain whose monomers experience only short-range interactions with each other and long-range interactions with the monomers of the unhybridized ss tails.

The chemical potentials μ_{pt} and μ_p are specified by the free energy per probe site of the surface, γ_{site}. In the 1:1 regime, when $\Sigma_0 > R_F^2 > r_F^2$, there is no mutual interaction between the probes or between the targets. The molar free energy of probe sites is

$$\gamma_{site} = \gamma_0 + x[\mu_{pt}^0 + N_{Av} G_{mush}(N - n) + N_{Av} G_{int}^{1:1}] + (1 - x)[\mu_p^0 + N_{Av} G_{mush}(n)] - TS[x]. \qquad (19)$$

Here γ_0 is the free-energy density of the bare surface whereas μ_{pt}^0 and μ_p^0 denote the chemical potentials of the hybridized and nonhybridized probes in the standard state. As noted before, the standard state of p is an ideal coil with no excluded volume interactions. The two G_{mush} terms allow for the excluded volume and screened electrostatic interactions as well as for the effect of the impenetrable wall. $G_{mush}(N - n)$ accounts for the monomer-monomer interactions of the unhybridized tail of pt whereas $G_{mush}(n)$ allows for the contribution of the unhybridized probe. $G_{int}^{1:1}$ reflects the electrostatic and excluded volume interactions between the hybridized target and its own probe. The mixing entropy per mol of p and pt sites is $S[x] = -R[x \ln x + (1 - x) \ln(1 - x)]$. The equilibrium condition $\mu_{pt} = \mu_p + \mu_t$ can be expressed in terms of the exchange chemical potential of the hybridized probe, $\mu_{pt}^{ex} = \mu_{pt} - \mu_p = \partial \gamma_{site}/\partial x$, as $\mu_{pt}^{ex} = \mu_t$. The hybridization isotherm, thus obtained, assumes the familiar Langmuir form

$$\frac{x_{eq}}{1 - x_{eq}} = c_t K_{pt}^{1:1} = c_t K_{pt}^0 \exp\left[-\frac{G_{mush}(N - n) + G_{int}^{1:1} - G_{mush}(n) - G_{coil}(N)}{kT} \right] \simeq c_t K_{pt}\left(\frac{n}{N}\right)^{2/5}. \qquad (20)$$

$K_{pt}^{1:1}$ is smaller than K_{pt} because of the effect of an impenetrable wall giving rise to the $(n/N)^{2/5}$ factor reflecting the reduction in the number of configurations available to the unhybridized tail of pt.

In the $\Sigma_0 > R_F^2 > r_F^2$ range the hybridization behavior is independent of x. As noted earlier, an x dependence is expected when $R_F^2 > \Sigma_0 > r_F^2$. We first discuss the 1:q regime occurring when $x < x_B$; γ_{site} in this range is similar to the one describing the 1:1 regime. The only difference is the replacement of $G_{int}^{1:1}$ by $G_{int}^{1:q}$, thus allowing for the interactions between a hybridized target and $q > 1$ probes. The hybridization isotherm as obtained from $\mu_{pt}^{ex} = \mu_t$ is

$$\frac{x_{eq}}{1 - x_{eq}} = c_t K_{pt}^{1:q} = c_t K_{pt}^0 \exp\left[-\frac{G_{mush}(N - n) + G_{int}^{1:q} - G_{mush}(n) - G_{coil}(N)}{kT} \right] \simeq c_t K_{pt}\left(\frac{n}{N}\right)^{2/5} \exp\left[-\frac{n}{N^{4/5}}(q - 1) \right]. \qquad (21)$$

As in the 1:1 regime, the hybridization isotherm is of the Langmuir form. The equilibrium constant, $K_{pt}^{1:q}$ is, however, smaller than $K_{pt}^{1:1}$ because $G_{int}^{1:q}$ is larger than $G_{int}^{1:1}$ by a factor of $q = R_F^2/\Sigma_0 = N^{6/5}a^2/\Sigma_0$.

When $\Sigma \leq R_F^2$ or $x \geq x_B = \Sigma_0/R_F^2 \simeq N^{-6/5}\Sigma_0/a^2$ the hybridized targets begin to crowd each other and form a brush. This crossover occurs at $x_{eq} = x_B$ corresponding to

$$c_B = \frac{\Sigma_0}{R_F^2 - \Sigma_0}\frac{1}{K_{pt}^{1:q}} = \frac{\Sigma_0}{R_F^2 - \Sigma_0}\frac{1}{K_{pt}}\left(\frac{N}{n}\right)^{2/5}\exp\left[\frac{n}{N^{4/5}}(q-1)\right]. \quad (22)$$

The γ_{site} term in the brush regime,

$$\gamma_{site} = \gamma_0 + x[\mu_{pt}^0 + N_{Av}G_{brush}(x) + N_{Av}G_{int}^B(x)] \\ + (1-x)[\mu_p^0 + N_{Av}G_{mush}(n)] - TS[x], \quad (23)$$

is distinctive in two respects. First, $G_{mush}(N-n)$ is replaced by an x dependent free energy of a chain in a brush, $G_{brush}(x)$. Second, the term allowing for the target-probe interactions, $G_{int}^B(x)$, is also a function of x. The hybridization isotherm, obtained as before, is

and $c_{50}^{1:q} = 1/K_{pt}^{1:q}$. In the opposite case, $x_B = \Sigma_0/R_F^2 < 1/2$, $x_{eq} = 1/2$ occurs in the brush regime and $c_{50}^B = 1/K_{pt}^B(x_{eq} = 1/2)$. The corresponding experimental guidelines assume a more useful form when considering the logarithm of c_{50}. In particular, these relate the range of expected target concentrations c_t, as given by $c_{50}^{1:q}$ or c_{50}^B, to ΔG_{pt}^0, n, N, and Σ_0

$$\ln c_{50}^{1:q} = \frac{\Delta G_{pt}^0}{RT} + \frac{2}{5}\ln\frac{N}{n} + N^{2/5}n\frac{a^2}{\Sigma_0} - n^{1/5}, \quad (25)$$

$$\ln c_{50}^B = \frac{\Delta G_{pt}^0}{RT} + \frac{1}{3}\ln\frac{2\Sigma_0}{n^{6/5}a^2} \\ + [N(1-2^{2/3}x_B^{2/3}) + 2n]\left(\frac{a^2}{2\Sigma_0}\right)^{2/3} - n^{1/5}. \quad (26)$$

The c_{50}^B can be significantly higher than $c_{50}^{1:q}$,

$$\ln\frac{c_{50}^B}{c_{50}^{1:q}} = [N(1-2^{2/3}x_B^{2/3}) + 2n]\left(\frac{a^2}{2\Sigma_0}\right)^{2/3} \\ - N^{2/5}n\frac{a^2}{\Sigma_0} + \frac{1}{3}\ln\frac{2\Sigma_0}{R_F^2} \gg 1, \quad (27)$$

$$\frac{x_{eq}}{1-x_{eq}} = c_t K_{pt}^B(x_{eq}) = c_t K_{pt}^0 \exp\left[-\frac{G_{brush}(x_{eq}) + G_{int}^B(x_{eq}) - G_{mush}(n) - G_{coil}(N)}{kT}\right] \\ \simeq c_t K_{pt}\left(\frac{n^{6/5}a^2 x_{eq}}{\Sigma_0}\right)^{1/3}\exp\left\{\frac{n}{N^{4/5}} - \left[Nx_{eq}^{2/3} - Nx_B^{2/3} + nx_{eq}^{-1/3}\right]\left(\frac{a^2}{\Sigma_0}\right)^{2/3}\right\}. \quad (24)$$

The $N^{1/5}$ term, arising from $G_{coil}(N)$ is expressed as $Nx_B^{2/3}(a^2/\Sigma_0)^{2/3}$ to underline the crossover behavior at x_B. By construction, this isotherm is only meaningful when $c_t > c_B$ so that $x > x_B$. It deviates strongly from the Langmuir form because of the x dependence of G_{brush} and G_{int}^B.

The complete "long-tail" hybridization isotherm for the $r_F^2 < \Sigma_0 < R_F^2$ case is obtained from Eqs. 21 and 24. In this isotherm, as in the interaction free Langmuir isotherm (Eq. 1), $x_{eq} \to 1$ as c_t increases. However, the two scenarios differ strongly with respect to the range of c_t involved (Fig. 2). The saturation in the long-tail case occurs at a much higher c_t. When x_{eq} vs. c_t curves of the two scenario are compared over a limited c_t range (Fig. 2 A), the long-tail isotherm is superficially similar to a Langmuir isotherm but with apparent saturation at $x_{eq} \ll 1$. A plot of x_{eq} vs. log c_t (Fig. 2 B) is necessary to visualize the differences in the saturation behavior.

A useful measure of the sensitivity of the DNA chip is the c_{50} corresponding to the target concentration, c_t, needed to obtain at equilibrium $x_{eq} = 1/2$ (13). The c_{50} also provides a rough estimate for the onset of saturation, as discussed earlier. In the 1:1 regime, where the hybridization follows a Langmuir isotherm, $c_{50}^{1:1} = 1/K_{pt}^{1:1}$. When $R_F^2 > \Sigma_0 > r_F^2$, we can distinguish between two scenarios. So long as $x_B = \Sigma_0/R_F^2 \geq 1/2$, $x_{eq} = 1/2$ is attained before the onset of the brush

because it is dominated by the factor exp $[N(1 - 2^{2/3}x_B^{2/3})(a^2/2\Sigma_0)^{2/3}]$. It is helpful to compare Eqs. 25 and 26 with the Langmuir isotherm of the "reference" state, Eq. 1, where $c_{50}^0 = 1/K_{pt}$. The guideline obtained, following the same procedure, is

$$\ln c_{50}^0 = \frac{\Delta G_{pt}^0}{RT} + \frac{n}{N^{4/5}} - n^{1/5}. \quad (28)$$

In this case c_{50}^0 is determined by n, N, and $\Delta G_{pt}^0/RT$. In marked contrast $c_{50}^{1:q}$ and c_{50}^B depend explicitly on Σ_0. The strong N dependence of c_{50}^B, as compared to $c_{50}^{1:q}$ and c_{50}^0, is illustrated in Fig. 3. The increase of c_{50}^B signals a corresponding loss of sensitivity.

To utilize these guidelines one needs ΔG_{pt}^0 as calculated using the nearest-neighbor model. However, to highlight the role of n as a design parameter, it is helpful to use the Wetmur approximation (52) where average values of the nearest-neighbor contributions are utilized. Accordingly, ΔG_{pt}^0 of perfectly matched probe-target pair, when the hybridization site is located within the target, is approximated by

$$\Delta G_{pt}^0 = (n-1)\overline{\Delta G_{nn}} + \overline{\Delta G_i} + 2\overline{\Delta G_e}, \quad (29)$$

where $\overline{\Delta G_{nn}}$, $\overline{\Delta G_i}$, and $\overline{\Delta G_e}$ are the average values corresponding to a nearest-neighbor pair, an initiation step and
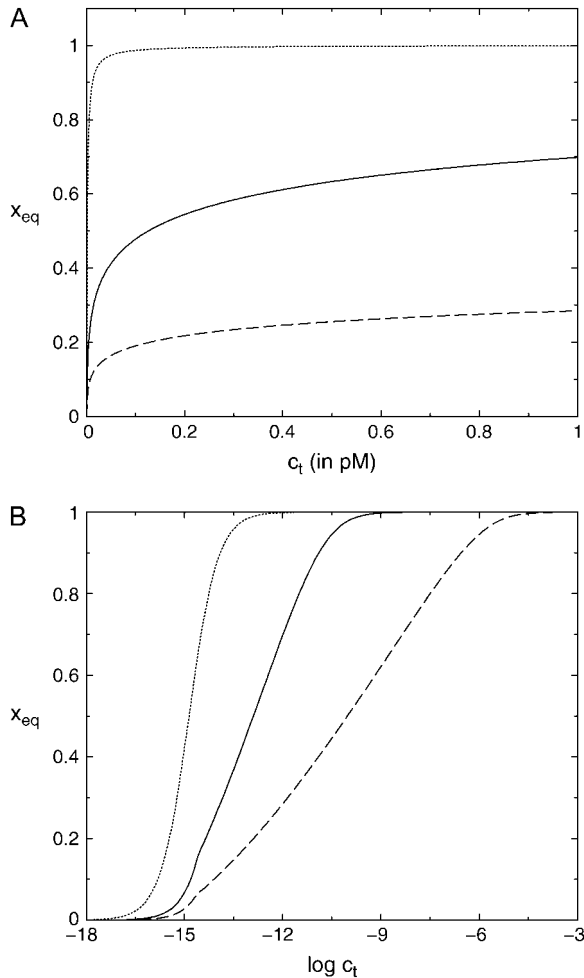
FIGURE 2 The hybridization isotherms as calculated using Eqs. 21 and 24 for the probe target pairs utilized by Guo et al.(5) with $\Sigma_0 = 2500$ Å^2 and $T = 30°C$. $N = 157$ (*solid line*), $N = 347$ (*dashed line*) and the reference state case calculated from Eq. 1 with $N = 157$ (*dotted line*). The x_{eq} vs. c_t curves are depicted in panel *A* for the range $0 \leq c_t \leq 1$ pM whereas x_{eq} vs. log c_t plots are depicted in panel *B* (-9 corresponds to 1 nM).

a dangling end. Wetmur estimated the nearest-neighbor contribution by $\overline{\Delta H_{nn}} = -8.0$ kcal/mol and $\overline{\Delta S_{nn}} = -21.5$ cal/mol K, the initiation term by a temperature independent $\overline{\Delta G_i} = 2.2$ kcal/mol and the dangling end contribution by $\overline{\Delta H_e} = -8.0$ kcal/mol and $\overline{\Delta S_e} = -23.5$ cal/mol K. Note that although useful, the Wetmur approximation erroneously predicts identical ΔG_{pt}^0 for all *pt* pairs with $N = n$.

BRUSH EFFECTS: KINETICS OF HYBRIDIZATION

Having obtained the equilibrium constants $K_{pt}^{1:1}$, $K_{pt}^{1:q}$, and $K_{pt}^B(x)$ for the hybridization at the surface we are now in a position to consider the corresponding rate constants. To this end we will assume, and later confirm, that the rate is reaction controlled. Again, for simplicity, we set numerical prefactors to unity, $v = a^3$ and $l_p = a$. It is necessary to recall
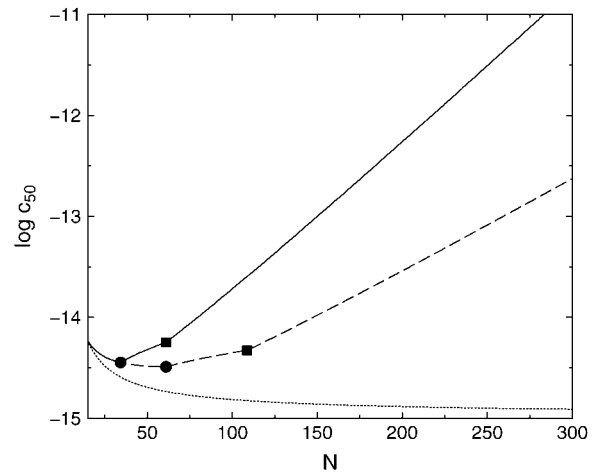
FIGURE 3 Plots of log c_{50}^B vs. *N* for the probes utilized by Guo et al. (5) with $\Sigma_0 = 2500$ Å^2 (*solid line*) and $\Sigma_0 = 5000$ Å^2 (*dashed line*). $T = 30°C$ and $n = 15$. The reference state log c_{50}^0 is plotted for comparison ($\cdots$). The circles correspond to the crossover between 1:1 and 1:*q* regimes whereas squares correspond to the crossover between 1:*q* and *B* regimes.

first the relevant features of the kinetics of oligonucleotide hybridization and of the desorption of polymers out of a brush.

As discussed in ''Design of oligonucleotide microarray experiments'', the reference state of our analysis is a layer of noninteracting probes bound to a passivated surface by long flexible spacers. We assume that the molecular mechanism of hybridization in this case is identical to the bulk one and that the kinetics follow the Langmuir rate law

$$\frac{dx}{dt} = k_h c_t (1 - x) - k_d x. \qquad (30)$$

In this regime the hybridization and denaturation rate constants, k_h and k_d, are independent of Σ_0 or *x* and approach their bulk values. At equilibrium $(dx/dt) = 0$ leading to $K_{pt} = k_h/k_d$ as required by detailed balance. In turn, the hybridization mechanism of free oligonucleotides in solution is thought to involve the steps outlined below (35,39,53,54). An approach and alignment of the single-stranded oligonucleotides is followed by the hybridization of a single basepair. A stable nucleus, comprising $n_c + 1$ basepairs, is formed by stepwise addition of hybridized pairs. Importantly, a ds sequence of $n \leq n_c$ is unstable. Once $n_c + 1$ is attained, the ds domain is rapidly ''zipped up''. For oligonucleotides comprising GC basepairs $n_c \simeq 2 - 3$ and the hybridization rate constant exhibits the form $k_h = \tau_h^{-1} \exp[-\Delta G_h^\#/RT]$. Here τ_h is a molecular timescale characterizing the formation of the last basepair of the nucleus whereas the activation free energy $\Delta G_h^\#$ reflects the formation of a ds nucleus of n_c basepairs plus the activation free energy for adding the next basepair. Importantly, the reaction is not diffusion controlled but involves a number of activation barriers associated with a corrugated free-energy profile (39). A rough estimate of $\Delta G_h^\#$ within the Wetmur

approximation (52) yields $\Delta G_{h}^{\#} \simeq n_{c}\overline{\Delta G}_{nn} + \overline{\Delta G}_{i} + 2\overline{\Delta G}_{e}$ indicating that $\Delta G_{h}^{\#}$ depends on n_{c} rather than n. This last point rationalizes a phenomenological result we will utilize later, namely k_{h} in high ionic strength solutions is

$$k_{h} \simeq 10^{6} M^{-1} s^{-1}, \qquad (31)$$

to within one order of magnitude and with a weak T dependence (39). This, together with the detailed balance requirement $K_{pt} = k_{h}/k_{d}$ yields

$$k_{d} \simeq 10^{6} \exp[\Delta G_{pt}^{0}/RT] \, s^{-1}. \qquad (32)$$

In terms of the Wetmur approximation k_{d} is expressed as $k_{d} \simeq \tau_{h}^{-1} \exp[(n - n_{c})\overline{\Delta G}_{nn}/RT]$. The activation barrier for denaturation involves, thus, the break up of $n - n_{c}$ basepairs so as to form an unstable ds domain. Importantly, for $15 \le n \le 25$, the denaturation life time at $37°C$ is measured in years.

At this point it is of interest to comment on a result, obtained from computer simulations, concerning the kinetics of desorption out of a brush (55). It concerns a planar brush formed from flexible and neutral chains with one terminal monomer experiencing a short-range attraction to the wall. The attraction was modeled as a well of width a, a monomer size, and depth G_{well}. In this system the expulsion rate constant is

$$k_{out} = \tau^{-1}(\Sigma)\exp[-G_{well}/RT], \qquad (33)$$

where $\tau(\Sigma)$ is the time required by the headgroup to diffuse across a distance $\Sigma^{1/2}$, corresponding to the innermost blob of the brush. Importantly, k_{out} although Σ dependent was found to be independent of N. Once the surface bond is broken, the expulsion of the chain out of the brush is driven by repulsive monomer-monomer interactions with neighboring chains. This last stage is a fast process and thus not rate controlling. The system studied in Wittmer et al. (55) differs from ours in two respects. First, in this study the attractive potential is laterally invariant, i.e., the surface is uniformly attractive. As a result, the reaction coordinate is the distance between the terminal end group and the surface z. In our case the attractive potential is localized at the immediate vicinity of the probe and the early steps of denaturation involve lateral separation of the two strands. Consequently the reaction coordinate at the vicinity of the surface is no longer z. Second, in Wittmer et al. (55), the barrier to adsorption is due to the brush. There is no barrier in the mushroom regime where the reaction is diffusion controlled. This is also the case in the brush regime when the terminal group resides within a distance $\Sigma^{1/2}$ from the surface. However, as noted earlier, the hybridization reaction in the bulk is not diffusion controlled. Accordingly, one should consider the possibility that the rate of hybridization at the surface is similarly not controlled by diffusion. In such a case the denaturation rate constant, corresponding to k_{out}, will be independent of both N and Σ.

In the following we will assume, and later confirm, that the rate of hybridization at the surface is reaction controlled rather than diffusion controlled. In quantitative terms, the implementation of the reaction control hypothesis involves three ingredients. First, we assume that the rate equation may be written as

$$\frac{dx}{dt} = k_{h}^{surf} c_{t}^{*}(1 - x) - k_{d}^{surf} x, \qquad (34)$$

where c_{t}^{*} is the local concentration of target hybridization sites in the vicinity of the probes; k_{h}^{surf} and k_{d}^{surf} denote the rate constants at the surface. In writing this equation we make a number of straightforward microscopic hypotheses. First, that the hybridization and denaturation reactions at the surface are, respectively, monomolecular and bimolecular. Second, the encounter probability between a probe and a target is proportional to c_{t}^{*}. Note that c_{t}^{*} is laterally invariant in the $1:q$ and brush regimes, thus implying that the diffusion is fast enough to ensure lateral homogeneity. The second ingredient requires a lengthier discussion. We will argue that k_{h}^{surf} differs from the corresponding bulk value whereas $k_{d}^{surf} = k_{d}$. The physical justification for this conjecture is as follows. The denaturation process is mostly local, reflecting reorganization of hydrogen bonds and stacking interactions (39). Accordingly, the breaking of the basepairs should not be influenced by the presence of the impenetrable wall. In contrast, we expect the wall to affect the hybridization process. In particular, the free-energy price for the approach and alignment of the single-stranded oligonucleotides should be lower because the entropy of the reacting chains at the impenetrable surface is lower. The last ingredient is the assumption that c_{t}^{*} for any x is equal to the equilibrium concentration of unhybridized terminal groups at the surface. In other words, the diffusion of chains is sufficiently fast in comparison to the hybridization reaction to ensure that a Boltzmann distribution is maintained. This condition is especially stringent in the brush regime, where inbound diffusion must overcome a potential barrier due to interactions with the previously tethered chains. The equilibrium condition requires that $c_{t}^{*}/c_{t} = \exp(-\Delta\mu/RT)$ where $\Delta\mu(x)$ is the difference between the chemical potential of a fully inserted chain and a free one. Altogether, for each of the three regimes

$$\frac{dx}{dt} = k_{h}^{surf}(i) c_{t}^{*}(i)(1 - x) - k_{d}x \equiv k_{h}^{i} c_{t}(1 - x) - k_{d}x, \quad (35)$$

where $k_{h}^{i} = k_{h}^{surf}(i) c_{t}^{*}(i)/c_{t}$ is the observable hybridization rate constant; $k_{h}^{surf}(i)$ and $c_{t}^{*}(i)$ specify, respectively, the values of k_{h}^{surf} and c_{t}^{*} in the i regime. At equilibrium the condition $(dx/dt) = 0$ yields

$$K_{pt}^{i} = \frac{k_{h}^{surf}(i)}{k_{d}} \frac{c_{t}^{*}(i)}{c_{t}} \qquad i = 1:1, \, 1:q, \, B. \qquad (36)$$

Because $K_{pt} = k_{h}/k_{d}$ the rate constants for the three regimes, $i = 1:1$, $1:q$ and B, are

$$k_{h}^{i} = k_{h} \frac{K_{pt}^{i}}{K_{pt}}, \qquad (37)$$

leading, up to numerical prefactors, to

$$k_h^B(x) \simeq k_h \left(\frac{n^{6/5} a^2 x}{\Sigma_0} \right)^{1/3} \exp\left[\frac{n}{N^{4/5}} - [N(x^{2/3} - x_B^{2/3}) \right.$$
$$\left. + nx^{-1/3}] \left(\frac{a^2}{\Sigma_0} \right)^{2/3} \right], \tag{38}$$

$$k_h^{1:q} \simeq k_h \left(\frac{n}{N} \right)^{2/5} \exp\left[-\frac{n}{N^{4/5}}(q-1) \right], \tag{39}$$

$$k_h^{1:1} \simeq k_h \left(\frac{n}{N} \right)^{2/5}. \tag{40}$$

Note that $k_h^{surf}(i)$ are independent of the regime i and larger than k_h. In particular, $k_h^{surf}(i)/k_h = n^{2/5} \exp(n/N^{4/5})$. The $n^{2/5}$ factor is due to the higher free energy of the probe as compared to that of the corresponding free oligonucleotide and the exponential term arises from probe-target interactions.

The results above were obtained assuming that the hybridization rate is controlled by the reaction rather than by the diffusion toward the surface. To check the consistency of this approach we consider the corresponding Damköhler number $Da = J_{reac}/J_{dif}$ (56). Here J_{reac} and J_{dif} are the maximal fluxes associated with the reaction and the inbound diffusion, assuming reaction control. Reaction control implies $Da \ll 1$. $J_{reac} = k_h^{surf} c_t^*/\Sigma_0$ is an upper bound on the reaction flux. The inbound flux of chain through the brush is $J_{dif} = c_t^* v_{barrier}$ where $v_{barrier}$ is the diffusion velocity of a single chain at the vicinity of the surface where the brush potential is essentially flat. Recent experimental results and a unified picture of theoretical models of J_{dif} are presented by Titmuss et al. (57). Altogether

$$Da = \frac{k_h^{surf}}{\Sigma_0 v_{barrier}}, \tag{41}$$

where $v_{barrier} = \alpha kT/\eta N a^2$. Here η is the solvent viscosity and α is a polymer specific numerical constant; α of ssDNA has not yet been determined but for flexible synthetic polymers $\alpha \simeq 0.1$. For water at 25°C $\eta = 0.89 \times 10^{-3}$ Nm^{-2}s. The Damköhler number at 25°C, when both fluxes are expressed in units of chains m^{-2}s^{-1}, is

$$Da = 0.13 \, n^{2/5} N \exp(n/N^{4/5})/\Sigma_0, \tag{42}$$

where we assumed $\alpha = 0.1$, $k_h = 10^6$ M^{-1}s^{-1}, $a = 6$ Å, and expressed Σ_0 in Å^2. For $100 \leq N \leq 600$, $n = 15$ and $T = 25$°C, the Damköhler number varies in the range $4 \times 10^{-2} \leq Da \leq 0.2$ when $\Sigma_0 = 1500$ Å^2 and $0.1 \leq Da \leq 0.5$ when $\Sigma_0 = 500$ Å^2. The variation of water viscosity in the range 0°C $\leq T \leq 70$°C affects the Da values at most by a factor 2. Accordingly, the assumption of reaction control of the hybridization rate is justified for typical values of N and Σ_0. It will, however, fail eventually for high N values. One

should note that the issue of reaction versus diffusion also arise for the diffusion from the bulk toward the surface. When the hybridization chamber is agitated this is not an issue and we will not discuss it further.

As required, the rate constants Eqs. 38–40 obey detailed balance and exhibit the proper crossover behavior. In particular, $k_h^i/k_d = K_{pt}^i$ as well as $k_h^B(x_B) = k_h^{1:q}$. The x dependence of k_h^B slows down the adsorption rate (Fig. 4); $k_h^B(x_{co}) = k_h/e$ is a possible measure for the onset of significant slow down due to the brush formation. In the limit of $N \gg 2n$ the $x^{-1/3}$ term is negligible and the onset occurs roughly at

$$x_{co} = \left[\frac{1}{N} \left(\frac{\Sigma_0}{a^2} \right)^{2/3} + x_B^{2/3} \right]^{3/2} \simeq x_B. \tag{43}$$

It thus affects the whole brush regime. The slower kinetics in the brush regime can affect the attained hybridization even after long hybridization periods (Fig. 5). This is of practical importance because samples of identical c_t but different N will vary in their signal intensity.

DISCUSSION

The relative size of the targets and probes is an important characteristic of oligonucleotide microarrays. When the two are of equal size, $N = n$, the onset of interaction between the probes is roughly set by the span of the probes as determined by n. In biology experiments the targets are much larger, $N \gg n$, and the onset of interactions is controlled by N. The progress of hybridization can give rise to crowding of the nonhybridized tails when $R_F^2 > \Sigma_0$. The polyelectrolyte
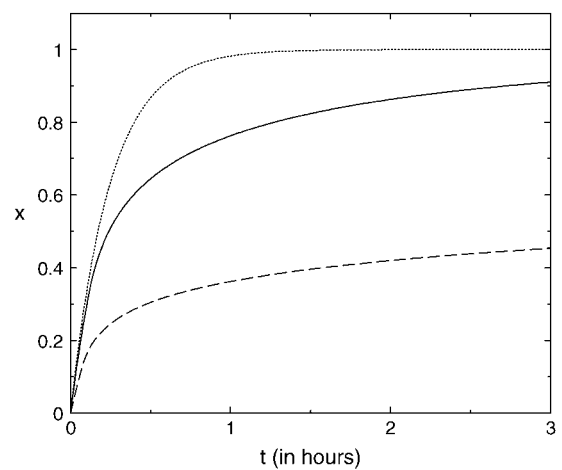

FIGURE 4 The hybridization kinetics, as described by a plot of x versus the time t in hours, for the probe target pairs of Guo et al. (5): $n = 15$, $T = 30$°C, $c_t = 1$ nM, and $\Sigma_0 = 5000$ Å^2. The $N = 157$ (*solid line*) and $N = 347$ (*dashed line*) curves are compared to the reference state case with $N = 157$ (*dotted line*).
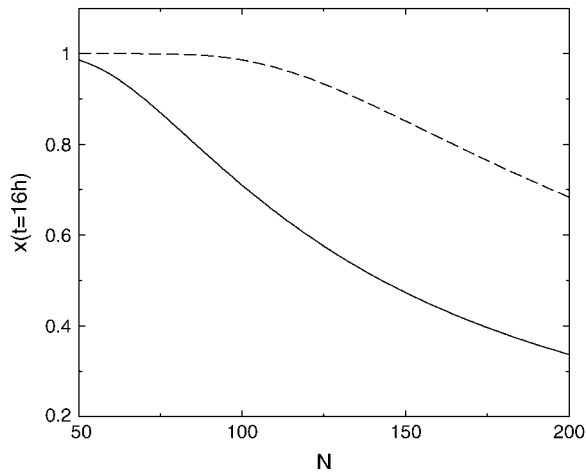
FIGURE 5 The hybridization fraction attained after $t_h = 16$ h as a function of N for the Affimetrix probe $p2$, $n = 25$, $T = 45°C$, $c_t = 0.1$ nM with $\Sigma_0 = 2500$ Å^2 (*solid line*) and $\Sigma_0 = 5000$ Å^2 (*dashed line*).

brush thus formed affects the hybridization isotherm and the rate equations. In particular, it lowers both the hybridization rate and the attainable hybridization for a given concentration of targets. It is important to allow for this effect in the design of DNA microarrays, in the formulating of the protocols of sample preparation and hybridization as well as in the analysis of the results. With regard to design of DNA chips the brush effect is important in choosing the desired density of oligonucleotide probes, or equivalently Σ_0. The brush effect will lower the fraction of probes that actually hybridize. As a result, the benefits of increasing the surface density of oligonucleotide probes diminish when the intended targets are long. When Σ_0 is set, these considerations suggest a criteria for tuning the length of the targets, N, as controlled by the choice of the PCR primers or of the fragmentation procedure. In particular, it is beneficial to shorten N so as to avoid crowding. When brush effects do occur the analysis of the results should allow for the ensuing deviations from the Langmuir behavior. This is an important point for the implementation of model-based algorithms.

Physical-chemistry-type experiments that aim to investigate the function of DNA microarrays tend to focus on the symmetric case of $N = n$. Our discussion highlights the merit of studying the kinetics and the equilibrium behavior in the asymmetric case, $N \gg n$. In this case it is of interest to correlate the hybridization behavior with measurements of the brush thickness.

Our analysis focused on the case of ssDNA targets so as to avoid complications due to the secondary structure of RNA molecules. The importance of the secondary structure of RNA targets, as used in gene expression experiments, is yet to be established because the effect of labeling by biotin is not well understood. The effect of the fragmentation on the kinetics of hybridization suggests, however, that a crowding effect of some sort is indeed involved.

APPENDIX A: THE VIRIAL COEFFICIENT AND THE CASE OF A BRUSH OF RODS

Consider first the second virial coefficient

$$v = \frac{1}{2} \int_0^\infty \left[1 - \exp(-U(r)/kT)\right] 4\pi r^2 dr, \quad (44)$$

for spherical monomers of radius a when their interactions are purely repulsive. In particular, the interaction potential, $U(r)$, comprises a hard-core repulsion together with a screened electrostatic repulsion, that is

$$\frac{U}{kT} = \begin{cases} \infty & r < a, \\ \dfrac{l_B}{r} \dfrac{\exp[-(r-a)/r_D]}{1 + a/r_D} & r > a. \end{cases} \quad (45)$$

Here r_D is the Debye screening length and l_B is the Bjerrum length (58). The hard-core contribution to v is $2\pi a^3/3$. The electrostatic contribution, assuming that $U/kT \ll 1$, is $2\pi l_B r_D^2$ and altogether

$$v = \frac{2\pi}{3} a^3 + 2\pi l_B r_D^2. \quad (46)$$

If one supplements the electrostatic repulsion U by a weak van der Waals attraction the first term assumes the form $2\pi a^3(1 - \theta/T)/3$ where θ is the θ-temperature (40) thus leading to Eq. 10. For 0.1 M of NaCl salt, $r_D = 10$ Å and assuming $a = 6$ Å we find that the electrostatic term dominates. When the salt concentration is 1 M the screening length diminishes to $r_D = 3$ Å and the two terms are comparable.

In the case of probes and targets of equal length, $n = N$, the probe layer consists of a mixture of single-stranded probes and hybridized, double-stranded ones. The associated interaction free energy for this case can be obtained (13) upon assuming, following Korolev et al. (59), that both adopt rod-like configurations of equal length $L = nb$ where $b \simeq 3.4$ Å is the contribution of a base or basepair to the length of the rod. The hybridized probes are rodlike because a dsDNA is rigid on the length scales of a typical probe ($10 \leq n \leq 30$). Viewing the unhybridized probes as rigid rods is an approximation justified, for the short probes, by two related observations. One is the tendency of ssDNA to form rigid domains of single-stranded helices due to stacking interactions (35,39,60). The second is that the persistence length attributed to ssDNA is comparable to the length of the probes. It is important, however, to stress that the configurations of ssDNA are not yet fully characterized. As noted in "Design of oligonucleotide microarray experiments", the reported values of the persistence length of ssDNA vary over a wide range 7.5 Å $\leq l_p \leq 35$ Å. In any case, the approximation of the brush height by L is sensible for short oligonucleotides with n such that $(nal_p)^{1/2} \simeq nb$. For reasonable values of l_p/a this condition is fulfilled for $n \simeq 15$. Similarly, the thermodynamic parameters of the stacking interactions are not fully established. With these reservations in mind, this picture provides a convenient approximation because it allows us to assign to the probe layer a unique thickness, independent of x. In particular, the thickness of the probe layer is comparable to L. The interaction free-energy density within the probe layer is accordingly, $F_{int} = vc^2$ where $c = n(1 + x)/\Sigma_0 L$ is the number concentration of monomers within the layer and the interaction free-energy density per unit area is

$$\gamma_{el} = 2\pi l_B r_D^2 \frac{n^2(1 + x)^2}{\Sigma_0^2 L}. \quad (47)$$

Accordingly, the overall free energy per probe site

$$\gamma_{site} = \gamma_0 + x\mu_{pt}^0 + (1 - x)\mu_p^0 + \Sigma_0 \gamma_{el}(x) + RT[x \ln x + (1 - x)\ln(1 - x)], \quad (48)$$

and the equilibrium condition $\mu_t = \mu_{pt}^{ex} = \partial \gamma_{site}/\partial x$ yields

$$\frac{x_{\text{eq}}}{1 - x_{\text{eq}}} = c_t K_{\text{pt}} \exp[-\Gamma(1 + x_{\text{eq}})], \quad (49)$$

with $\Gamma = 4\pi n^2 l_B r_D^2 / \Sigma_0 L$. This recovers, up to a factor of 2, results we obtained earlier using the box approximation for the solution of the Poisson-Boltzmann equation (13). The isotherm obtained above differs from the ''brush isotherm'' because the chain elasticity does not play a role and the layer thickness does not exhibit an x dependence.

APPENDIX B: EFFECT OF CHAIN SELF-AVOIDANCE ON THE HYBRIDIZATION CONSTANTS

The Flory approximation as used in the text overestimates both the elastic and interaction free energies. Another delicate point concerns the entropy of the free ends. At the same time, the Flory approximation is known to be robust and its performance has been studied showing relatively mild deviation from the exact results obtained by SCF theory (24). With these points in mind it is of interest to confirm the results obtained utilizing the Alexander-Flory approximation by a more rigorous approach. In the following we present exact results concerning $K_{\text{pt}}^{1:1}$. In particular, the alternative derivation allows for the chain self-avoidance while ignoring the small correction due to interactions between the hybridized ds domain and unhybridized tail of the target. To this end we utilize the partition function of a self-avoiding chain (61,62). The partition function $Z_{\text{coil}}(N)$ of a free self-avoiding chain of N monomers is

$$Z_{\text{coil}}(N) = z^N N^{\gamma - 1} \quad (50)$$

where z is the model-dependent effective partition function of a monomer, and γ is a universal configurational exponent. For a self-avoiding chain with a terminal monomer anchored to an impenetrable planar surface, a ''mushroom'', the partition function is

$$Z_{\text{mush}}(N) = z^N N^{\gamma_1 - 1}, \quad (51)$$

where γ_1 is a different universal configurational exponent.

When a probe and a target hybridize, the ds domain can be envisioned as a rigid rod with a partition function

$$Z_{\text{rod}}(n) = z_{\text{rod}}^n = z_0^{2n} \exp[-\Delta G_{\text{pt}}^0(n)/RT]. \quad (52)$$

Here, z_{rod} is the partition function of a pair of hybridized monomers, z_0 is partition function of a single monomer in an ideal Gaussian coil, n is number of basepairs in the ds domain, and $\Delta G_{\text{pt}}^0(n)$ is the free-energy difference between the rigid ds and ideal coil ss domains. The free-energy G is related to the partition function Z by $G = -RT \ln Z$.

The hybridization constant K_{pt} in a solution of targets and probes whose respective lengths are N and $n \ll N$ is

$$K_{\text{pt}} = \exp\{-[G_{\text{rod}}(n) + G_{\text{coil}}(N - n) - G_{\text{coil}}(N) - G_{\text{coil}}(n)]/RT\}. \quad (53)$$

Using Eqs. 50, 52, and 53, we obtain

$$K_{\text{pt}} = \frac{Z_{\text{rod}}(n) Z_{\text{coil}}(N - n)}{Z_{\text{coil}}(n) Z_{\text{coil}}(N)} = \left(\frac{N - n}{N}\right)^{\gamma - 1}$$
$$\times n^{1-\gamma} \left(\frac{z_0}{z}\right)^{2n} \exp[-\Delta G_{\text{pt}}^0(n)/RT] \approx K_{\text{pt}}^0 n^{1-\gamma} \left(\frac{z_0}{z}\right)^{2n}, \quad (54)$$

where $K_{\text{pt}}^0 = \exp[-\Delta G_{\text{pt}}^0/RT]$ as introduced earlier.

For the hybridization at a surface in the 1:1 regime

$$K_{\text{pt}}^{1:1} = \exp\{-[G_{\text{rod}}(n) + G_{\text{mush}}(N - n) - G_{\text{coil}}(N)$$
$$- G_{\text{mush}}(n) - \delta S_{\text{rod}}]/RT\}. \quad (55)$$

Here, $\delta S_{\text{rod}} \equiv \ln(\beta)$ is the reduction in the rod entropy due to its attachment to the surface. The specific value of β, of order unity, depends on the length and flexibility of the spacer. In the simplest case, of a short flexible spacer, the surface eliminates half of the space available to a free rod in the solution, thus yielding $\beta = 1/2$. Equations 50, 51, and 55 lead to

$$K_{\text{pt}}^{1:1} = \beta \frac{Z_{\text{rod}}(n) Z_{\text{mush}}(N - n)}{Z_{\text{mush}}(n) Z_{\text{coil}}(N)} = \beta \left(\frac{N - n}{n}\right)^{\gamma_1 - 1} N^{1-\gamma} \left(\frac{z_0}{z}\right)^{2n}$$
$$\times \exp[-\Delta G_0(n)/RT] \approx \beta K_{\text{pt}}^0 N^{1-\gamma} \left(\frac{N}{n}\right)^{\gamma_1 - 1} \left(\frac{z_0}{z}\right)^{2n}. \quad (56)$$

The ratio of hybridization constants at the surface and in solution, as determined from Eqs. 54 and 56 is

$$\frac{K_{\text{pt}}^{1:1}}{K_{\text{pt}}} = \beta \left(\frac{n}{N}\right)^{\gamma - \gamma_1} \quad N \gg n. \quad (57)$$

The values of $\gamma \approx 1.167$ and $\gamma_1 \approx 0.695$ were obtained using field theoretical methods and numerical calculations (61,62). Therefore, $\gamma - \gamma_1 \approx 0.47$ is in close agreement with $K_{\text{pt}}^{1:1}/K_{\text{pt}} = (n/N)^{2/5}$, Eq. 20.

REFERENCES

1. Graves, D. J. 1999. Powerful tools for genetic analysis come of age. *Trends Biotechnol.* 17:127–134.

2. Wang, J. 2000. From DNA biosensors to gene chips. *Nucleic Acids Res.* 28:3011–3016.

3. Lockhart, D. J., and E. A. Winzeler. 2000. Genomics, gene expression and DNA arrays. *Nature.* 405:827–836.

4. Heller, M. J. 2002. DNA microarray technology: devices, systems and applications. *Annu. Rev. Biomed. Eng.* 4:129–153.

5. Guo, Z., R. A. Guilfoyle, A. J. Thiel, R. Wang, and L. M. Smith. 1994. Direct fluorescence analysis of genetic polymorphism by hybridization with oligonucleotide arrays on glass supports. *Nucleic Acids Res.* 22:5456–5465.

6. Prix, L., P. Uciechowski, B. Böckmann, M. Giesing, and A. J. Schuetz. 2002. Diagnostic biochip array for fast and sensitive detection of K-*ras* mutations in stool. *Clin. Chem.* 48:428–435.

7. Chan, V., D. J. Graves, and S. McKenzie. 1995. The biophysics of DNA hybridization with immobilized oligonucleotide probes. *Biophys. J.* 69:2243–2255.

8. Livshits, M. A., and A. D. Mirzabekov. 1996. Theoretical analysis of the kinetics of DNA hybridization with gel-immobilized oligonucleotides. *Biophys. J.* 71:2795–2801.

9. Vainrub, A., and M. B. Pettitt. 2002. Coulomb blockage of hybridization in two-dimensional DNA arrays. *Phys. Rev. E Stat. Nonlin. Soft Matter Phys.* 66:041905.

10. Bhanot, G., Y. Louzoun, J. Zhu, and C. DeLisi. 2003. The importance of thermodynamic equilibrium for high throughput gene expression arrays. *Biophys. J.* 84:124–135.

11. Held, G. A., G. Grinstein, and Y. Tu. 2003. Modeling of DNA microarray data by using physical properties of hybridization. *Proc. Natl. Acad. Sci. USA.* 100:7575–7580.

12. Zhang, L., M. F. Miles, and K. D. Aldape. 2003. A model of molecular interactions on short oligonucleotide microarrays. *Nat. Biotechnol.* 21:818–821.

13. Halperin, A., A. Buhot, and E. B. Zhulina. 2004. Sensitivity, specificity, and the hybridization isotherms of DNA chips. *Biophys. J.* 86:718–730.

14. Halperin, A., A. Buhot, and E. B. Zhulina. 2004b. Hybridization isotherms of DNA chips and the quantification of mutation studies. *Clin. Chem.* 50:2254–2262.

15. Forman, J. E., I. D. Walton, D. Stern, R. P. Rava, and M. O. Trulson. 1998. Thermodynamics of duplex formation and mismatch discrimination on photolithographically synthesized oligonucleotide arrays. *ACS Symp. Ser.* 682:206–228.

16. Okahata, Y., M. Kawase, K. Niikura, F. Ohtake, H. Furusawa, and Y. Ebara. 1998. Kinetic measurements of DNA hybridization on an oligonucleotide-immobilized 27-MHz quartz crystal microbalance. *Anal. Chem.* 70:1288–1296.

17. Steel, A. B., T. M. Herne, and M. J. Tarlov. 1998. Electrochemical quantitation of DNA immobilized on gold. *Anal. Chem.* 70: 4670–4677.

18. Georgiadis, R., K. P. Peterlinz, and A. W. Peterson. 2000. Quantitative measurements and modeling of kinetics in nucleic acid monolayer films using SPR spectroscopy. *J. Am. Chem. Soc.* 122:3166–3173.

19. Nelson, B. P., T. E. Grimsrud, M. R. Liles, R. M. Goodman, and R. M. Corn. 2001. Surface plasmon resonance imaging measurements of DNA and RNA hybridization adsorption onto DNA microarrays. *Anal. Chem.* 73:1–7.

20. Dai, H., M. Meyer, S. Stepaniants, M. Ziman, and R. Soughton. 2002. Use of hybridization kinetics for differentiating specific from non-specific binding to oligonucleotide microarrays. *Nucleic Acids Res.* 30:e86.

21. Kepler, T. B., L. Crosby, and K. T. Morgan. 2002. Normalization and analysis of DNA microarray data by self consistency and local regression. *Genome Biol.* 3:0037.1–0037.12.

22. Peterson, A. W., L. K. Wolf, and R. M. Georgiadis. 2002. Hybridization of mismatched or partially matched DNA at surfaces. *J. Am. Chem. Soc.* 124:14601–14607.

23. Hekstra, D., A. R. Taussig, M. Magnasco, and F. Naef. 2003. Absolute mRNA concentrations from sequence-specific calibration of oligonucleotide arrays. *Nucleic Acids Res.* 31:1962–1968.

24. Milner, S. T. 1991. Polymer brushes. *Science.* 251:905–914.

25. Halperin, A., M. Tirrell, and T. P. Lodge. 1992. Tethered chains in polymer microstructures. *Adv. Polym. Sci.* 100:31–71.

26. Rühe, J., M. Ballauff, M. Biesalski, P. Dziezok, F. Grohn, D. Johannsmann, N. Houbenov, N. Hugenberg, R. Konradi, S. Minko, M. Motornov, R. R. Netz, et al. 2004. Polyelectrolyte brushes. *Adv. Polym. Sci.* 165:77–150.

27. Pincus, P. 1991. Colloid stabilization with grafted polyelectrolytes. *Macromolecules.* 24:2912–2919.

28. Borisov, O. V., T. M. Birshtein, and E. B. Zhulina. 1991. Collapse of grafted polyelectrolyte layer. *J. Phys. II.* 1:521–526.

29. Su, H.-J., S. Surrey, S. E. McKenzie, P. Fortina, and D. J. Graves. 2002. Kinetics of heterogeneous hybridization on indium tin oxide surfaces with and without an applied potential. *Electrophoresis.* 23:1551–1557.

30. Rosenow, C., R. M. Saxena, M. Durst, and T. R. Gingeras. 2001. Prokaryotic RNA preparation methods useful for high density array analysis: comparison of two approaches. *Nucleic Acids Res.* 29: E112.

31. Affymetrix. 2004. GeneChip Expression Analysis. Technical Manual. Available at http://www.affymetrix.com/support/technical/manuals.affx [Online].

32. Pirrung, M. C. 2002. How to make a DNA chip? *Angew. Chem. Int. Ed. Engl.* 41:1277–1289.

33. Southern, E., K. Mir, and M. Shchepinov. 1999. Molecular interactions on microarrays. *Nat. Genet.* 21:5–9.

34. Naef, F., and M. Magnasco. 2003. Solving the riddle of the bright mismatches: labeling and effective binding in oligonucleotide arrays. *Phys. Rev. E Stat. Nonlin. Soft Matter Phys.* 68:011906.

35. Cantor, C. R., and P. R. Schimmel. 1980. Biophysical Chemistry. W. H. Freeman, New York, NY.

36. Smith, S. B., Y. J. Cui, and C. Bustamante. 1996. Overstretching B-DNA: the elastic response of individual double-stranded and single-stranded DNA molecules. *Science.* 271:795–799.

37. Strick, T. R., M.-N. Dessinges, G. Charvin, N. H. Dekker, J.-F. Allemand, D. Bensimon, and V. Croquette. 2003. Stretching of macromolecules and proteins. *Rep. Prog. Phys.* 66:1–45.

38. Mills, J. B., E. Vacano, and P. J. Hagerman. 1999. Flexibility of single-stranded DNA: use of gapped duplex helices to determine the persistence lengths of poly(dT) and poly(dA). *J. Mol. Biol.* 285:245–257.

39. Turner, D. H. 2000. Chap.8 Conformational Changes. *In* Nucleic Acids: Structures, Properties and Functions. V. A. Bloomfield, D. Crothers, and I. Tinoco, Jr. University Science Books, Sausalito, CA.

40. Rubinstein, M., and R. H. Colby. 2003. Polymer Physics. Oxford University Press, Oxford, UK.

41. SantaLucia, J., and D. Hicks. 2004. The thermodynamics of DNA structural motifs. *Annu. Rev. Biophys. Biomol. Struct.* 33:415–450.

42. SantaLucia, J. 1998. A unified view of polymer, dumbbell, and oligonucleotide DNA nearest-neighbor thermodynamics. *Proc. Natl. Acad. Sci. USA.* 95:1460–1465.

43. Peyret, N., P. A. Seneviratne, H. T. Allawi, and J. SantaLucia. 1999. Nearest-neighbor thermodynamics and NMR of DNA sequences with internal A.A, C.C, G.G, and T.T mismatches. *Biochemistry.* 38:3468–3477.

44. Peyret, N., and J. SantaLucia, Jr. HyTer, Version 1.0. Wayne State University, Detroit, MI. Available at http://ozone2.chem.wayne.edu/hyther/hytherm1main.html [Online].

45. Alexander, S. 1977. Adsorption of chain molecules with a polar head—a scaling description. *J. Phys. (Paris).* 38:983–987.

46. Birshtein, T. M., and E. B. Zhulina. 1984. Conformations of star-branched macromolecules. *Polym.* 25:1453–1461.

47. DiMarzio, E. A. 1965. Proper accounting of conformations of a polymer near a surface. *J. Chem. Phys.* 42:2101–2106.

48. De Gennes, P. G. 1979. Scaling Concepts in Polymer Physics. Cornell University Press, Ithaca, NY .

49. Evans, D. F., and H. Wennerström. 1994. The Colloid Domain. VHC, New York, NY.

50. Birshtein, T. M., Yu. V. Liatskaya, and E. B. Zhulina. 1990. Theory of supermolecular structure of polydisperse block copolymers. 1. Planar layers of grafted chains. *Polym.* 31:2185–2196.

51. Moore, W. J. 1972. Physical Chemistry. Longman, London, UK.

52. Wetmur, J. G. 1991. DNA probes: applications of the principles of nucleic acid hybridization. *Crit. Rev. Biochem. Mol. Biol.* 26:227–259.

53. Craig, M. E., D. M. Crothers, and P. Doty. 1971. Relaxation kinetics of dimer formation by self complementary oligonucleotides. *J. Mol. Biol.* 62:383–392.

54. Pörschke, D., and M. Eigen. 1971. Co-operative non-enzymatic base recognition. III. Kinetics of the helix-coil transition of the oligoribouridylic·oligoriboadenylic acid system and of oligoriboadenylic acid alone at acidic pH. *J. Mol. Biol.* 62:361–364.

55. Wittmer, J., A. Johner, J. F. Joanny, and K. Binder. 1994. Chain desorption from semidilute polymer brush: a Monte Carlo simulation. *J. Chem. Phys.* 101:4379–4390.

56. Blanch, H. W., and D. S. Clark. 1996. Biochemical Engineering. Marcel Dekker, New York, NY.

57. Titmuss, S., W. H. Briscoe, I. E. Dunlop, G. Sakellariou, N. Hadjichristidis, and J. Klein. 2004. Effect of end-group sticking energy on the properties of polymer brushes: comparing experiment and theory. *J. Chem. Phys.* 121:11408–11419.

58. Fowler, R., and E. A. Gugenheim. 1960. Statistical Thermodynamics. Cambridge, UK.

59. Korolev, N., A. P. Lyubartsev, and L. Nordenskiöld. 1998. Application of polyelectrolyte theories for analysis of DNA melt-ing in the presence of Na^+ and Mg^{2+} Ions. *Biophys. J.* 75:3041–3056.

60. Buhot, A., and A. Halperin. 2004. Effects of stacking on the configurations and elasticity of single-stranded nucleic acids. *Phys. Rev. E Stat. Nonlin. Soft Matter Phys.* 70:020902.

61. Duplantier, B. 1989. Statistical mechanics of polymer networks of any topology. *J. Stat. Phys.* 54:581–680.

62. Eisenriegler, E., K. Kremer, and K. Binder. 1982. adsorption of polymer chains at surfaces: scaling and Monte Carlo analyses. *J. Chem. Phys.* 77:6296–6320.